Available online at www.sciencedirect.com
SCIENCE DIRECT
Chemical Engineering and Processing 45 (2006) 113–123
Chemical Engineering and Processing
www.elsevier.com/locate/cep

LLECMOD: A Windows-based program for hydrodynamics simulation of liquid–liquid extraction columns

Menwer M. Attarakih [a], Hans-Jörg Bart [a,*], Luis Lagar G. [a], Naim M. Faqir [b]

[a] *University of Kaiserslautern, Faculty of Mechanical and Process Engineering, Institute of Thermal Process Engineering, PO Box 3049, D-67653 Kaiserslautern, Germany*
[b] *University of Jordan, Faculty of Engineering and Technology, Chemical Engineering Department, 11942 Amman, Jordan*

Received 21 May 2004; received in revised form 30 September 2004; accepted 23 March 2005
Available online 29 August 2005

Abstract

The simulation of liquid–liquid extraction columns based on a droplet population balance approach provides a useful means for getting more insight into the transient and the steady state behavior of such an extremely important unit operation. This numerical simulation is carried out based on a recently developed algorithm for solving the population balance equation. The algorithm is implemented via a computer program called liquid–liquid extraction column module (LLECMOD). The LLECMOD is designed in a flexible way that allows the user to define the breakage and coalescence frequencies, droplet terminal velocity, and the other internal geometrical details of the column. The user input dialog makes the LLECMOD a user-friendly program that enables the user to select the simulation parameters and functions in an easy way. The program is reinforced by a parameter estimation package for the droplet coalescence models. In this work, a sample of small laboratory and pilot plant simulations as compared to the experimental data is presented as carried out by the LLECMOD.

Keywords: LLECMOD; RDC column; Population balances; Hydrodynamics

1. Introduction

The simulation of chemical engineering processes is now widely used to shed some light on the dynamic or steady state performance as well as equipment scale up of many types of unit operation equipment. This is because in most cases the actual running of the equipment is very expensive or sometimes prohibitive due to safety reasons even at the laboratory scale. An important unit operation in chemical engineering is liquid–liquid extraction that finds many significant applications in mining, petroleum, food and pharmaceutical industries [1]. The hydrodynamics as well as the mass transfer in such unit operations is fundamentally influenced by the behavior of the dispersed phase consisting of populations of distributed rather than lumped characteristics in droplet phase space. Consequently, the natural framework of modelling of such dispersed phase processes is based on the population balance [2–4]. Although such modelling framework is rich in the information it furnishes, it is still expensive from a computational point of view since the full population balance models are normally integral partial differential equations (IPDE) of stretched type [5]. These IPDEs have only a limited number of analytical solutions [6,7] that are in most cases strongly simplified and hence are physically unrealistic. Consequently, for realistic liquid–liquid extraction column (LLEC) simulation based on population balance modelling, it is inevitable to seek numerical solutions. In such cases the need for numerical solutions imposes two levels of difficulties due to the convective, droplet breakage and coalescence events occurring simultaneously. The convective process in dispersed phase systems is actually dominant when compared to the axial dispersion and hence sharp front profiles describing the number or volume concentration distributions are expected to develop along the spatial coordinate

* Corresponding author. Tel.: +49 631 205 2414; fax: +49 631 205 2119.
E-mail address: bart@mv.uni-kl.de (H.-J. Bart).
URL: http://www.uni-kl.de/LS-Bart/.

0255-2701/$ – see front matter © 2005 Elsevier B.V. All rights reserved.
doi:10.1016/j.cep.2005.03.012

in the direction of flow. At the same time the evolution of these distributions is governed by the breakage and coalescence mechanisms involving linear integral expressions for breakage and non-linear ones for droplet coalescence. These issues are fully discussed by Attarakih et al. [6] where an efficient numerical algorithm based on the generalized fixed-pivot technique and the central differencing schemes of Kurganov and Tadmor [8] is presented and extensively tested. For user-friendly implementation of such a numerical algorithm we introduce in this work the basics of a Windows-based computer program called liquid–liquid extraction column module (LLECMOD). The basic feature of this program is to provide the simulation of the hydrodynamics of LLECs based on the population balance approach for both transient and steady state through an interactive Windows input dialogue as well as a parameter estimation package for droplet coalescence models based on small scale laboratory devices. The LLECMOD is not restricted to a certain type of liquid–liquid extraction column since it is built in the most general form that allows the user to input the various droplet interaction functions. These functions include droplet terminal velocity taking into account the swarm effect, slowing factor due to column geometry, the breakage frequency and daughter droplet distribution, the coalescence frequency and the axial dispersion coefficients. A sample problem on basis of the performance of a RDC column is given. However, other column types can easily be treated, e.g. Kühni columns, when using adapted correlations [9].

2. The mathematical model

The population balance equation (PBE) based on the number concentration distribution along the column can be formulated as follows [4]:

$$\frac{\partial n}{\partial t} + \frac{\partial F}{\partial z} = \frac{\partial}{\partial z}\left(D_\mathrm{d}\frac{\partial n}{\partial z}\right) + \frac{Q_\mathrm{d}}{A_\mathrm{c}}\left(\frac{n^\mathrm{feed}}{v_\mathrm{f}}\right)\delta(z - z_\mathrm{d}) + \rho\{n, v\} \quad (1)$$

where $n(v; z, t)\delta v = N(t, z)f(v)\delta v$ is the average number concentration associated with droplets having a volume between $v \pm \delta v$ at the time instant t and column height z, $N(t, z)$ is the total number concentration and $f(v)$ is the droplets number density. The convective flux of these droplets along the column of a constant cross-sectional area, A_c, is represented by $A_\mathbf{c}F\delta v = A_\mathrm{c}U_\mathrm{d}n\delta v$, where U_d is the velocity of the dispersed phase relative to the column walls. The first term on the right-hand side of Eq. (1) represents the axial dispersion of the dispersed phase due to the non-ideal flow in which a random movement of the fluid on the microscopic level is superimposed on the main flow [10]. This is assumed to follow Fick's law with a dispersion coefficient, D_d, and is distinguished from the forward mixing effect due to the droplet velocity distribution that is taken into account by the convective term [11]. The second term on the right-hand side represents a number concentration rate of droplets entering as a feed of volumetric flow rate, Q_d, at the level z_d of the column. The positive direction of flow coincides with the dispersed phase flow from z_d to the top of the column. Note that the feed distribution is represented mathematically by a point source through the use of the Dirac delta function [12]. The last term on the right-hand side of Eq. (1) represents the net rate of the number of droplets generated by breakage and coalescence events per unit volume and is reported in detail by Attarakih et al. [6].

The boundary conditions are greatly simplified since the dispersed and the continuous phases are included in the mathematical model given by Eq. (1) as point sources. Accordingly, the Danckwert's boundary conditions based on the discussion of Wilburn [13] could be written by considering the LLEC to behave like a closed vessel between 0^+ and column height H:

$$0 = \max(F, 0) - D_\mathrm{d}\frac{\partial n}{\partial z} \quad \text{at } z = 0 \quad (2)$$

$$0 = -\min(F, 0) + D_\mathrm{d}\frac{\partial n}{\partial z} \quad \text{at } z = H \quad (3)$$

$$n(v; z, t) = n_0(v; z) \quad \forall z \in [0, H] \quad (4)$$

The first step in the numerical solution of these equations is to project the infinite system (with respect to droplet volume or diameter) of IPDEs given by Eq. (1) onto a finite system of partial differential equations (PDE) using the generalized fixed pivot technique. The idea in this technique is to divide the internal droplet coordinate (volume) into contiguous finite subdomains covering the range of this internal coordinate. In each subdomain, the total volume concentration is obtained by integrating the volume concentration distribution with respect to volume (diameter) over the boundaries of this subdomain. This local volume concentration is then concentrated at a single point in this subdomain called the fixed-pivot, x_i, and is given by

$$\varphi_i(z, t) = \int_{v_{i-1/2}}^{v_{i+1/2}} v(v)n(v; z, t)\,\mathrm{d}v = v(x_i)N_i(z, t), \quad i = 1, 2, \ldots, M_x \quad (5)$$

This replaces the IPDE given by Eq. (1) by M_x finite number of PDEs that are non-linearly coupled through the convective and the source terms. These PDEs are then discretized based on upwind and central differencing schemes resulting in the following semi-discrete formulation:

$$\frac{\mathrm{d}\varphi_{i,l}}{\mathrm{d}t} + \frac{F_{i,l+1/2} - F_{i,l-1/2}}{\Delta z_l} = \frac{D_\mathrm{d}\partial\varphi_i/\partial z|_{l+1/2} - D_\mathrm{d}\partial\varphi_i/\partial z|_{l-1/2}}{\Delta z_l} + \frac{Q_\mathrm{d}}{A_\mathrm{c}}\frac{\varphi_i^\mathrm{feed}}{v_\mathrm{f}}\frac{\delta_{l,l_\mathrm{d}}}{\Delta z_l} + \rho(\boldsymbol{\varphi}_l, \boldsymbol{d}), \quad i = 1, 2, \ldots, M_x, \quad l = 1, 2, \ldots, L \quad (6)$$

The numerics are treated in detail by Attarakih et al. [6]. In addition, the source term takes into account the conservation of any two integral properties, u_1 and u_2 and is given by

$$\rho(\varphi) = \begin{pmatrix} \varphi^{\mathrm{T}}[(\omega \cdot \Psi^{\langle 1\rangle})\varphi] \\ \varphi^{\mathrm{T}}[(\omega \cdot \Psi^{\langle 2\rangle})\varphi] \\ \cdots \\ \varphi^{\mathrm{T}}[(\omega \cdot \Psi^{\langle M_x\rangle})\varphi] \end{pmatrix} - \varphi^{\mathrm{T}} \cdot [\omega(\zeta \cdot \varphi)] + A[\Gamma \cdot \varphi] \tag{7}$$

where

$$A_{i,k} = \begin{pmatrix} [\pi_{i,i}^{\langle m\rangle} - 1] \\ \pi_{i,k}^{\langle m\rangle} \end{pmatrix}, \quad i = 1, 2, \ldots, M_x, \quad k = i, i+1, \ldots, M_x \tag{8}$$

$$\pi_{i,k}^{\langle m\rangle} = \int_{d_{i-1}}^{d_i} \gamma_i^{\langle i-1\rangle}(d) \left[\frac{u_m(d_i)}{u_m(d_k)}\right] \beta_n(d|d_k)\delta d + \int_{d_i}^{\min(d_k, d_{i+1})} \gamma_i^{\langle i\rangle}(d) \left[\frac{u_m(d_i)}{u_m(d_k)}\right] \beta_n(d|d_k)\delta d \tag{9}$$

$$\zeta_k = \frac{1}{u_m(x_k)} \tag{10}$$

$$\Psi_{k,j}^{\langle i\rangle} = \begin{cases} \left[1 - \frac{1}{2}\delta_{k,j}\right] \frac{u_m(x_i)}{u_m(x_j)u_m(x_k)} \gamma_i^{\langle i-1\rangle}(x_k + x_k) & \text{if } d_{i-1}^3 \le x_j + x_k < d_{i-1}^3 \\ \left[1 - \frac{1}{2}\delta_{k,j}\right] \frac{u_m(x_i)}{u_m(x_j)u_m(x_k)} \gamma_i^{\langle i\rangle}(x_k + x_k) & \text{if } d_i^3 \le x_j + x_k < d_{i+1}^3 \end{cases} \tag{11}$$

$$\Gamma_i = \Gamma(d_i, \phi(t, z)), \quad i = 1, 2, , \ldots, M_x \tag{12}$$

$$\omega_{i,k} = \omega(d_i, d_k, \phi(t, z)), \quad i, k = 1, 2, , \ldots, M_x \tag{13}$$

$\gamma_i^{\langle i-1\rangle}$ and $\gamma_i^{\langle i\rangle}$ are triangular functions defined in [6]. Note that the above mathematical model conserves the total droplet number and volume by setting $u_1 = 1$ and $u_2 = v$.

3. User input data and functions

The above discrete formulation requires a grid structure input for both droplet diameter and column height: d_i, $i = 1, 2, \ldots, M_x$; z_l, $l = 1, 2, \ldots, L$; the breakage frequency function $\Gamma(d_i, \phi(z_l, t))$; the coalescence frequency $\omega(d_i, d_j, \phi(z_l, t))$, and the droplet rise velocity. All these parameters and functions must be defined in a user supplied input module in FORTRAN90 format. All the following input features can

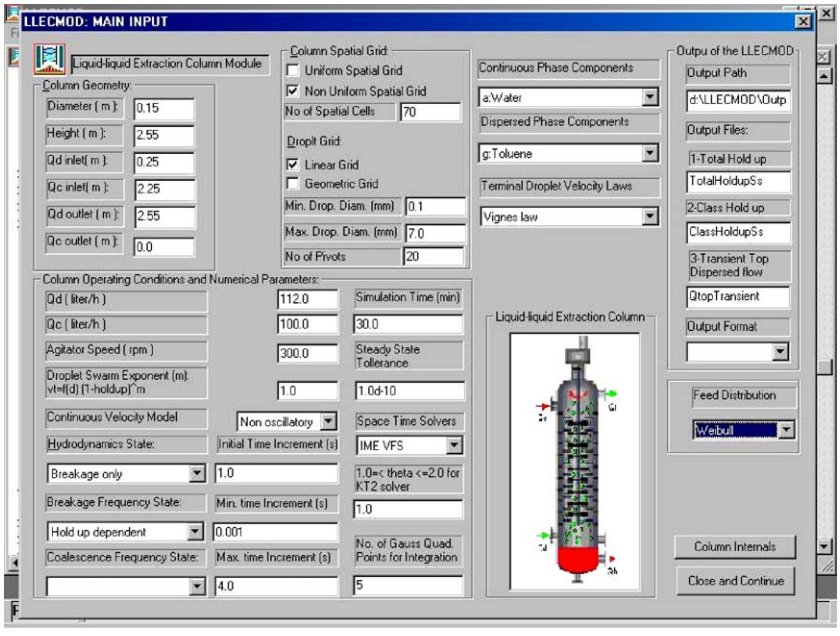

Fig. 1. The main input dialog of the LLECMOD showing the input of the present sample problem.

be selected in the main input frame (see Fig. 1), which also determines the output results.

3.1. Grids generation

The grid structure depends on the column geometry as shown in Fig. 1 as well as the minimum and maximum droplet diameters prevailing in the column. The program provides two types of grids for both column height and droplet diameter. For droplet diameter geometric and uniform droplet discretizations are available:

$$d_{i-1/2} = d_{\min}\left(\frac{d_{\max}}{d_{\min}}\right)^{(i-1)/M_x}, \quad i = 1, 2, \ldots, M_x + 1 \tag{14}$$

$$d_{i-1/2} = d_{\min} + \left(\frac{d_{\max} - d_{\min}}{M_x}\right)(i-1), \quad i = 1, 2, \ldots, M_x + 1 \tag{15}$$

For the column height the uniform grid structure has the same form as that given by Eq. (15) by replacing d with z. However, the non-uniform grid structure is constructed by a combination of uniform grids to produce a relatively fine structure around the dispersed and continuous phases inlets where permanent discontinuities appear. This provides sharp resolution of these discontinuities at steady state conditions without excessive increase in the number of grid points.

3.2. Dispersed and continuous phases chemical components

The physical properties required for the evaluation of droplet transport and interactions (breakage and coalescence) are loaded from a simple database containing the chemical components for the dispersed and continuous phases. However, the user could add the physical properties for any new chemical component by editing the files: LLECMOD\CompData.

3.3. Inlet feed distribution

The inlet feed distribution appearing in Eq. (1) can be supplied by the user in either two ways: First by representing the discrete data in tabulated form, where the feed distribution is normalized internally according to the relation:

$$\varphi_i^{\text{feed}} = \frac{\bar{\varphi}_{\text{i}}\,\Delta d_i}{\sum_{i=1}^{M_x}\bar{\varphi}_{\text{i}}\,\Delta d_i} \tag{16}$$

The second form of the feed input is in the form of three frequently used distributions to fit the liquid–liquid distributors or droplet distributions in agitated columns: the normal, log normal and Weibull distributions.

3.4. The terminal droplet velocity

The LLECMOD has four terminal droplet velocity laws that can be chosen by the user. These velocity laws are: Klee and Treybal [14], Vignes [15], Grace [16] and the rigid sphere law [17]. If the user does not choose any of these laws, the LLECMOD automatically chooses by default the suitable velocity law based on the selection chart detailed in the book of Godfrey and Slater [9]. Moreover, if the user has a specific velocity law he can add it to the user input module as a FORTRAN90 code. This may be to take into account the droplet swarm effect in a function proportional $(1-\Phi)^m$ [18].

3.5. The continuous phase velocity models

The continuous phase velocity models required to calculate the dispersed phase velocity U_{d} are shown in Table 1. The first velocity model corresponds to the interface level control as shown in Fig. 2. In this control scheme the outlet continuous flow rate is manipulated to control the position of the interface at the top of the column. The velocity model corresponding to this scheme shows an oscillatory behavior in the dispersed phase hold-up as reported both experimentally [19] and theoretically [6,20]. The second velocity model assumes that the continuous phase is at steady state and hence it is not applicable for transient simulations, while the third velocity model is based on the control scheme shown in Fig. 2 by manipulating the inlet continuous phase flow rate. This resulting oscillation in the dispersed phase hold-up could be explained as follows [20]: At the instant of introducing the dispersed phase at z_{d} the outlet flow rate of the continuous phase increases immediately because it is displaced by the dispersed phase ($\phi_{\text{d}} + \phi_{\text{c}} = 1$), at the same time the dispersed phase hold-up is propagated along the column causing an increase in the top flow rate, Q_{t}. At $z = z_{\text{d}}$ and according to

Table 1
Available continuous phase velocity models

Continuous phase velocity model	Reference
1. Oscillatory: $U_{\text{c}} = \frac{Q_{\text{t}}}{A_{\text{c}}} - \alpha_{\text{c}}\frac{Q_{\text{c,in}}}{A_{\text{c}}} - \alpha_{\text{d}}\frac{Q_{\text{d,in}}}{A_{\text{c}}} - \int_{d_{\min}}^{d_{\max}} v(d)U_{\text{r}}(d,\phi,\boldsymbol{P})n(d;z,t)\delta d$, $Q_{\text{t}} = \int_{d_{\min}}^{d_{\max}} v(d)U_{\text{r}}(d;\phi(H,t),\boldsymbol{P})n(d;H,t)\delta d$	[3]
2. Steady state: $U_{\text{c}} = \alpha_{\text{c}}\frac{Q_{\text{c}}}{A_{\text{c}}(1-\phi)} + \frac{D_{\text{c}}}{1-\phi}\frac{\partial\phi}{\partial z}$	[12]
3. Nonoscillatory: $U_{\text{c}} = \frac{Q_{\text{t}}}{A_{\text{c}}} - \alpha_{\text{c}}\frac{Q_{\text{c,in}}}{A_{\text{c}}} - \alpha_{\text{d}}\frac{Q_{\text{d,in}}}{A_{\text{c}}} - \int_{d_{\min}}^{d_{\max}} v(d)U_{\text{r}}(d,\phi,\boldsymbol{P})n(d;z,t)\delta d$ with $Q_{\text{c,in}} = Q_{\text{t}} + \frac{1}{1-\phi_{\text{e}}}Q_{\text{c,out}} - Q_{\text{d}}$, $\alpha_{\text{c}} = \begin{cases} 1, & z \le z_{\text{c}} \\ 0, & z > z_{\text{c}} \end{cases}$ and $\alpha_{\text{d}} = \begin{cases} 1, & z \le z_{\text{d}} \\ 0, & z > z_{\text{d}} \end{cases}$	[6]

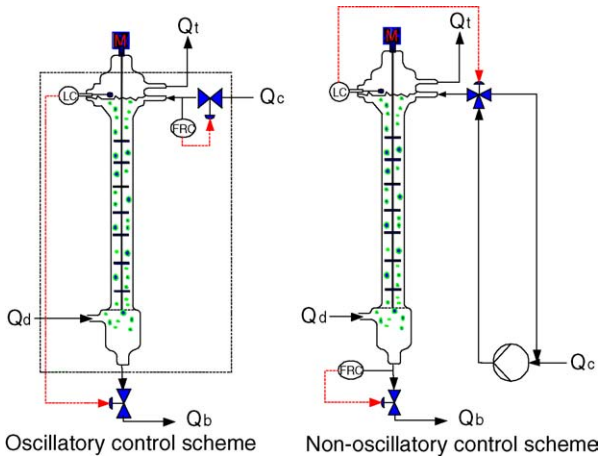

Fig. 2. Conventional and improved dispersed phase level controls [19].

the velocity model 1 shown in Table 1, $Q_{c,out} = A_c U_c$ starts to decrease to satisfy the total volume balance (note that $n(d; z < z_d, t) = 0$ away from flooding conditions). As a result this reduction in the continuous phase flow rate at the bottom of the column will decrease the dispersed phase hold-up according to $U_d = U_r - U_c$.

Accordingly, this decrease in the dispersed phase hold-up will propagate along the column and hence causing the top flow to decrease. This causes the continuous flow rate at the bottom to increase and hence the dispersed phase hold-up will increase again and the process repeats itself with decreasing amplitude that is damped when the steady state is approached.

The non-oscillatory velocity model gets rid of this resonance behavior by keeping the continuous phase flow rate at the bottom of the column at a constant value and hence it allows the inlet flow rate to vary according to: $Q_{c,in} = Q_t + \frac{1}{1-\phi_e} Q_{c,out} - Q_d$ [6]. This is found to eliminate completely the oscillatory behavior of the dispersed phase hold-up since its magnitude at the base of the column is maintained constant as long as Q_d is constant.

3.6. Axial dispersion coefficients

The axial dispersion coefficients, D_c and D_d for the dispersed and continuous phases, respectively, are defined in the user input module as functions D_c and D_d using FORTRAN90. These coefficients are allowed only to vary with the column height in the present version of LLECMOD.

3.7. Breakage frequency and daughter droplet distribution

The breakage frequency function $\Gamma(d, U_d, \phi(z, t))$ can be easily defined in the user input module using FORTRAN90 format. For the case that the breakage frequency is independent of the dispersed phase hold-up or the dispersed phase velocity it is called separable; that is, $\Gamma = \Gamma(d)$. In this case we choose from the input menu: *breakage frequency state/hold-up independent*, which is the default. On the other hand, if $\Gamma = \Gamma(d, \phi(z, t))$, we choose: *breakage frequency state/hold-up dependent*.

3.8. The coalescence frequency

The coalescence frequency function $\omega(d, d', \phi(z, t))$ is defined in the user input module using FORTRAN90. For the case that the coalescence frequency is independent of the dispersed phase hold-up, it is called separable; that is, $\omega = \omega(d, d')$. In this case we choose from the input menu: *coalescence frequency state/hold-up independent*, which is the default. On the other hand, if $\omega = \omega(d, d', \phi(z, t))$ we choose: *coalescence frequency state/hold-up dependent*.

4. Droplet phase space–time solvers

The LLECMOD provides three droplet phase space–time solvers to discretize droplet diameter, column height and time as shown in Table 2. The algorithms on which these solvers are built are fully described and extensively tested by Attarakih et al. [6]. The user can choose from the drop-down menu provided by the input dialogue, the suitable solver with IME FVS as the default one. The minimum and maximum time steps, the final simulation time, the steady state tolerance, and the total variation diminishing (TVD) parameter θ for IME KT2 solver can also be chosen by the user from the input dialogue. The value of the TVD parameter ranges from 1 to 2 with value 2 for the least dissipative behavior while the value 1 guarantees a non-oscillatory scheme.

5. The LLECMOD output

The output from the LLECMOD is of two types: the first one is graphical output consisting of the most important simulation results. These are the inlet feed distribution, the relative

Table 2
Available phase space–time solvers in LLECMOD

Solver	Order	Description
IME FVS	First order in time and space	Upwind differencing with flux vector splitting with implicit Euler method
IME KT1	First order in time and space	Non-oscillatory central differencing with implicit Euler method
IME KT2	First order in time and second order in space	Non-oscillatory central differencing scheme with implicit Euler method

Table 3
RDC column geometry

Column diameter (m)	0.15
Stator diameter (m)	0.105
Rotor diameter (m)	0.090
Compartment height (m)	0.030
Column height (m)	2.550
Dispersed phase inlet (m)	0.250
Continuous phase inlet (m)	2.250

droplet velocity taking into account the slowing factor K_v, the hold-up along the column, the mean droplet diameter (Sauter diameter) along the column, and the droplet volume distribution at selected positions along the column. The second output is written to three output files: the total hold-up and the mean droplet diameter of the dispersed phase along the column, the droplet volume distribution along the column, and the transient top flow rate.

6. Coalescence parameters estimation package

Droplet coalescence is sensitive to hydrodynamics, physico-chemical properties, interfacial dynamics and mass transfer. Up to now it is not possible to present a correlation to predict the coalescence rate. However, basic experiments in a Venturi-tube have shown that the coalescence probability of droplets strongly depends on the droplet size, the hold-up and system properties [21,22]. Therefore, it is not possible to introduce a correlation for predicting the droplet coalescence independent of solving the population balance equation describing this phenomenon. This is because droplet coalescence is more complex than droplet breakage, which is weakly affected by the turbulent structure of the continuous phase. The physico-chemical properties of the continuous phase and the turbulent fluctuations play an important role in droplet coalescence. It is believed that droplet coalescence occurs if the random contact time between any two coalescing droplets exceeds the time required for the complete intervening film drainage and rupture [23]. Coulaloglou and Tavlarides [23] expressed the coalescence frequency as a product of collision rate and coalescence efficiency based on the kinetic theory of gases and obtained the following expression:

$$\omega(d, d', \phi_y, \boldsymbol{P}) = c_1 \frac{\varepsilon^{1/3}}{1+\phi}(d+d')^2(d^{2/3}+d'^{2/3})^{1/2} \times \exp\left(-\frac{c_2 \mu_c \rho_c \varepsilon}{\sigma^2(1+\phi)^3}\left(\frac{dd'}{d+d'}\right)^4\right) \quad (17)$$

To determine the unknown constants: c_1 and c_2, the droplet coalescence was investigated in a small laboratory-scale device, which consists of five compartments (see also Table 3) in total having an active height and diameter of 0.15 m. Droplet size distributions were measured at the inlet and the outlet of the short segment RDC column. The experiments in this small device were carried out with the saturated system water/*n*-butyl acetate. The phase flow throughput was set in a range between 13.9 and 27.8 mL/s. The rotational speed was within a range of 150–300 rpm.

To estimate c_1 and c_2, an integrated optimization package was developed to solve this inverse problem based on the above mathematical model that is simplified (by neglecting the axial dispersion) for a short RDC segment, which is geometrically similar to that of a pilot scale plant. The program calculates the unknown coalescence constants within a chosen coalescence model (Eq. (17)). These constants are obtained by an inverse solution of the PBE for this segment based on minimizing the sum of squares of errors according to the following objective function:

$$\chi^2(\boldsymbol{c}) = [\boldsymbol{F} - \tilde{\boldsymbol{F}}(\boldsymbol{c})]^{\mathrm{T}}[\boldsymbol{F} - \tilde{\boldsymbol{F}}(\boldsymbol{c})] \quad (18)$$

where $\boldsymbol{c}$ is the unknown coalescence constants vector $\boldsymbol{c} = [\,c_1 \quad c_2\,]$.

Therefore the simulated steady state outlet cumulative distribution $\tilde{\boldsymbol{F}}$ is fitted to the experimental one, $\boldsymbol{F}$, by varying the coalescence parameters vector $\boldsymbol{c}$. This procedure is carried out using the Rosenbrock method [24], which uses only the function values and utilizes simple bounds on the estimated constants. Moreover, the optimization algorithm is reinforced by a multivariate statistical tool to estimate the confidence intervals for the calculated constants. The performance of the Rosenbrock algorithm was also tested against the standard IMSL subroutine DBCPOL based on the direct search complex algorithm [25].

7. Sample problem

In this section a sample problem is considered to illustrate the basic features of the LLECMOD and the coalescence parameters estimation package including the main input parameters and the user input functions. For this purpose the steady state experimental data for the hydrodynamics of a laboratory scale RDC column whose dimensions are shown in Table 3 was utilized first to estimate the coalescence parameters appearing in Eq. (17). The chemical system used is the EFCE test system: water/*n*-butyl acetate whose physical properties are available online (http://www.dechema.de/Extraktion). Due to the relatively low interfacial tension of this system, the droplet coalescence as well as breakage has an important effect on the column hydrodynamics.

Additionally, the experimentally correlated droplet transport functions, the breakage frequency, and the daughter droplet distribution based on the work of Modes [26] and Schmidt et al. [27] were used. These were determined based on single droplet experiments carried out in a column segment having one compartment of total height 0.03 m. The droplet rise velocities and the breakage probability functions are determined using digital image processing, while the

axial dispersion coefficient of the dispersed phase is determined using residence time analysis for a monodispersion of droplets of specified diameters [26]. The dispersion coefficient of the continuous phase was after a correlation of Steiner and Hartland [28]. As a suitable velocity law based on the selection chart detailed in the book of Godfrey and Slater [18], the Klee and Treybal [14] velocity law was used to estimate the terminal droplet velocity, which was then multiplied by $(1-\phi)$ to take into account the droplet swarm effect [18]. The slowing factor, K_v, of Modes [26] adapted after a correlation of Godfrey and Slater [29] and the axial dispersion coefficient, D_d, is

$$K_v(d, N^*) = 1-1.037(N^{*3}D_R^5)^{0.12} - 0.62\left(\frac{d}{D_s - D_R}\right)^{0.44} \quad (19)$$

$$\frac{D_d}{U_d H} = 0.0138 + 8.26\times 10^{-7}\left(\frac{N^* D_R}{U_d}\right)^{3.3} \quad (20)$$

where N^* is the rotor speed (s^{-1}), D_R and D_s are the rotor and stator diameters, respectively, whose values are shown in Table 3.

The droplet breakage frequency and the daughter droplet distribution are correlated based on single droplet experiments and are given by

$$\Gamma(d,\phi) = P_r(d, N^*)\frac{|U_d(d,\phi)|}{H_c} \quad (21)$$

The breakage probability, P_r, is correlated with the system physical properties and the energy dissipation in the following form [26] adapted from a correlation of Cauwenberg et al. [30]:

$$\frac{p_r}{1-p_r} = 1.2\times 10^{-6}\left[\frac{\rho_c^{0.8}\mu_c^{0.2} d D_R^{1.6}(2\pi)^{1.8}}{\sigma} \times (N^{*1.8} - N_{crit}^{*1.8})\right]^{2.88} \quad (22)$$

where $N_{R,crit}$ is the critical rotor speed below which the breakage probability falls to zero and H_c is the RDC compartment height.

The daughter droplet distribution is assumed to follow the beta distribution, which is given by [30]:

$$\beta_n(d|d') = 3\vartheta(\vartheta-1)\left[1-\left(\frac{d}{d'}\right)^3\right]^{\vartheta-2}\frac{d^2}{d'^3} \quad (23)$$

where ϑ is the mean number of daughter droplets produced upon breakage of mother droplet of diameter d'. It is experimentally correlated and found dependent on the energy dissipation and having a value ≥ 2.

First, the coalescence constants appearing in Eq. (17) were estimated for the system water/*n*-butyl acetate using the coalescence parameter estimation package described in Section 6 at different rotational speeds. The detailed internal RDC column geometry is shown in Fig. 3 which is based on the values indicated in Table 3. Fig. 4 shows the results of fitting the steady state cumulative volume distribution at the outlet of the five-compartment RDC column using 30 experimental data points, where very good agreement between the experimental and predicted densities is evident. The mean

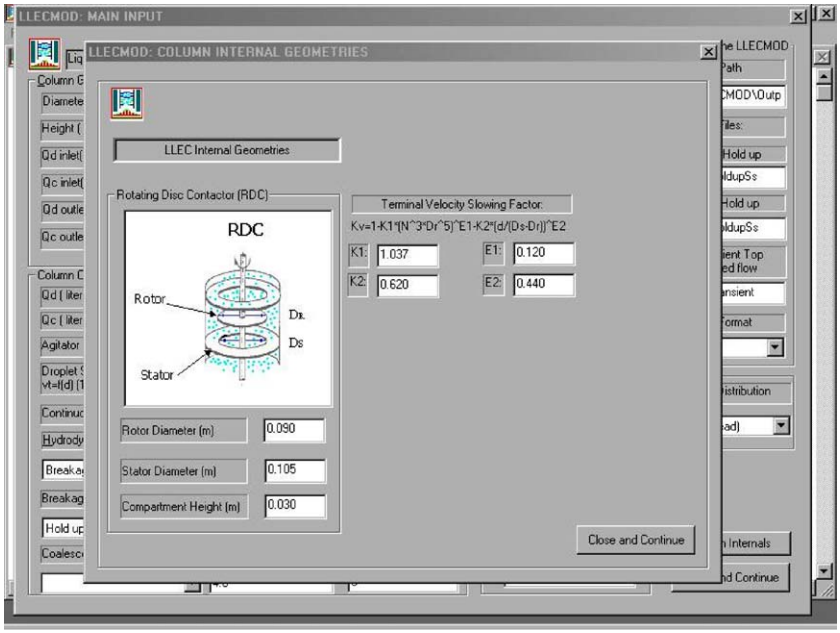

Fig. 3. The LLECMOD input dialog for internal RDC column geometries.

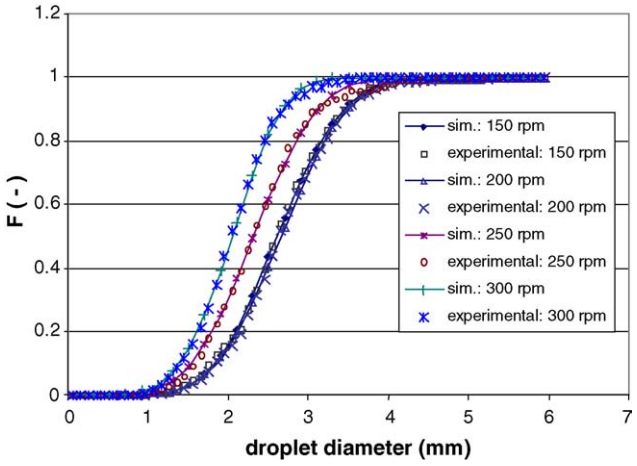

Fig. 4. Comparison between the predicted and experimental cumulative volume distribution at the outlet of a short segment RDC column at steady state for the system water/*n*-butyl acetate.

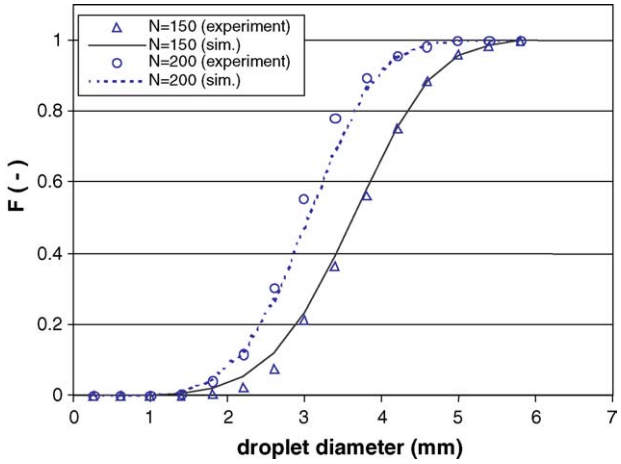

Fig. 5. Comparison between the predicted and experimental cumulative volume distribution at the outlet of a pilot plant RDC column at steady state using the system water/*n*-butyl acetate.

values of the estimated parameters are: $c_1 = 0.0694 \pm 0.002$ and $c_2 = 1.3 \times 10^{11}\,\mathrm{m}^{-2} \pm 1 \times 10^{6}\,\mathrm{m}^{-2}$ corresponding to a 95% confidence interval, where the objective function (Eq. (18)) is not very sensitive to changes in the values of the constant c_2, which may vary ±50%, which agrees to the reported results in the published literature [31]. Moreover, the values of these constants are in the same order of magnitude as that reported in the literature [31,32].

Second, the estimated parameters above were used to simulate a pilot plant RDC column with total active height of 1.76 m where its characteristic dimensions are shown in Table 3. In all the numerical simulations the inlet feed distribution is based on the measured values. The numerical integration is carried out until steady state using the IME FVS solver with grid having a dimension of 70 × 20, where doubling of the grid size shows no principal differences in the predicted results. The minimum droplet diameter is chosen to lie above the critical droplet diameter for stable droplets, according to [27]:

$$N_{\mathrm{crit}} = 0.016\frac{D_{\mathrm{R}}^{-2/3}\eta_{\mathrm{d}}d^{-4/3}}{(\rho_{\mathrm{c}}\rho_{\mathrm{d}})^{1/2}} + \left[\left(0.008\frac{D_{\mathrm{R}}^{-2/3}\eta_{\mathrm{d}}d^{-4/3}}{(\rho_{\mathrm{c}}\rho_{\mathrm{d}})^{1/2}}\right)^2 + 0.127\frac{\sigma}{\rho_{\mathrm{c}}D_{\mathrm{R}}^{4/3}d^{5/3}}\right]^{0.5} \quad (24)$$

The user input parameters using the LLECMOD main input dialog are shown in Fig. 1. The input parameters and data shown in Figs. 1 and 3 are echoed on the LLECMOD working window before the space–time integrator is started. Once all the input is echoed the user is asked to choose the droplet phase-space solver. When the final simulation time is exceeded or the steady state tolerance is achieved the LLECMOD presents the results in graphical form showing the most important data for the simulation such as the hold-up, Sauter diameter and droplet size distribution as well as a summary of the simulation results displayed in a separate window. The graphics library used to generate the output is an improved and modified version of the SIGRAPH library provided with the Compaq visual FORTRAN version 6.6.

Fig. 5 compares the cumulative droplet volume distributions at the top of the column using two agitator speeds: 150 and 200 rpm. It is evident that the two steady state distributions are well predicted and the volumetric distribution is shifted to the left as the rotor speed is increased indicating the increase of the breakage rate. This fact is elucidated by closely examining the hold-up profiles in Fig. 6, where the hold-up at 200 rpm rotor speed is increased due to the increase of small droplets residence time. Although the steady state hold-up profiles were not accurately predicted especially at the bottom of the column, the general trend iss predicted.

Fig. 7 shows again that the droplet coalescence is dominant at the 150 rpm rotational speed as indicated by the increase of the mean droplet diameter along the column height. As the rotor speed is increased to 200 rpm, the two interaction droplet mechanisms (breakage and coalescence) are almost balanced with slight dominance of droplet breakage. This fact is reflected by referring to Eq. (17), where the coalescence efficiency decreases as the energy input increases. Moreover, the steady state discontinuities due to the dispersed and continuous phases inlets are highly resolved due to the non-uniform spatial grid used in the simulation.

Fig. 8 shows the evolution of the dispersed phase flow rate at the top of the column using the oscillatory and non-oscillatory velocity models given in Table 1. It is clear that the two velocity models are only identical at steady state where the conservation of mass is exactly satisfied.

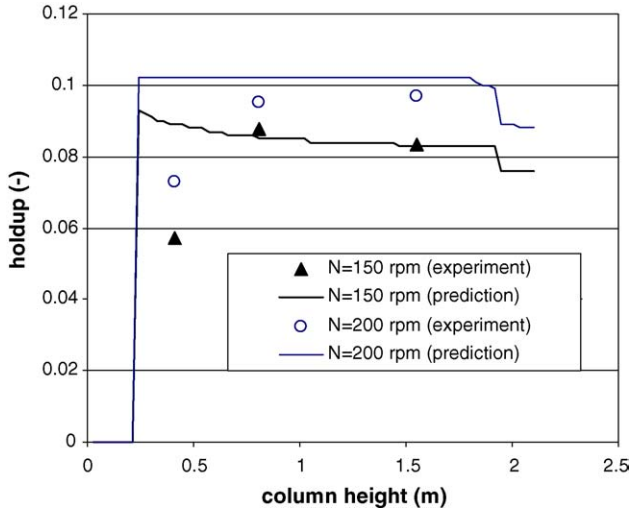

Fig. 6. Comparison between the predicted and simulated hold-up profiles in a pilot plant RDC column at different rotational speeds at steady state using the system water/*n*-butyl acetate.

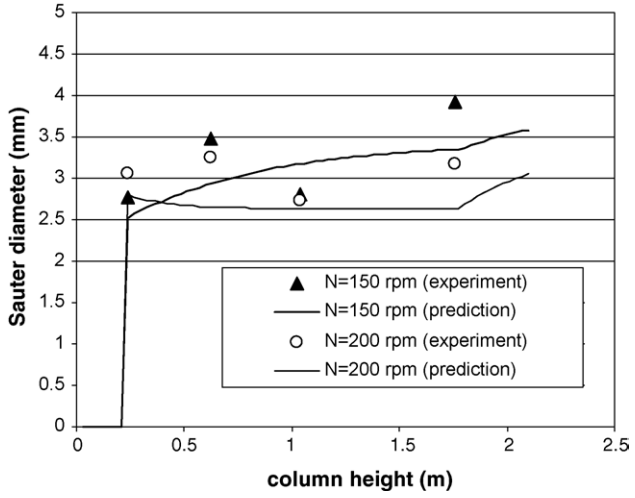

Fig. 7. Comparison between the predicted and simulated Sauter droplet diameter in a pilot plant RDC column at different rotational speeds at steady state using the system water/*n*-butyl acetate.

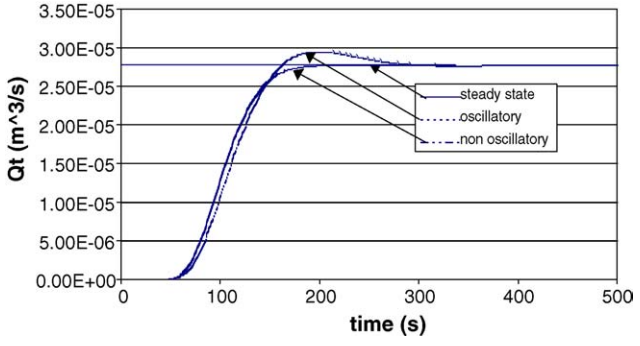

Fig. 8. Comparison between the oscillatory and non-oscillatory velocity models in a pilot plant RDC column at 200 rpm rotor speed using the system water/*n*-butyl acetate.

The CPU time requirements on a PC of 700 MHz speed for this case is 128 s using a steady state tolerance of 10^{-10}; however, this time could be reduced if this tolerance is reduced. The performance of the other solvers has been extensively tested by Attarakih et al. [6] and was found to produce identical results at steady state. However, for transient simulations it was found that the first order solvers (IME FVS and IME KT1) suffer from numerical diffusion due to the steep moving fronts of the droplets hold-up of different sizes. This numerical diffusion is greatly reduced when the second-order solver (IME KT2) is used and thus the moving fronts can be captured correctly.

8. Conclusions

In this paper the numerical algorithm developed by Attarakih et al. [6] was exploited successfully to develop the basic features of a Windows-based program LLECMOD for the hydrodynamics simulation of general liquid–liquid extraction columns as well as the parameter estimation package for the droplet coalescence model. These packages are based on the population balance approach to model the hydrodynamics of interacting liquid–liquid dispersions taking into account droplet transport as well as the breakage and coalescence. The user-friendly input dialogue and the user functions input module make the program very general and simple to use. For steady state simulation purposes, the IME FVS solver is found to be the best when very sharp hold-up profiles are not expected to occur. However, the accuracy of the spatial second-order solver (IME KT2) makes it very attractive for transient simulations without appreciable increase in the CPU time [6].

Appendix A. Nomenclature

$\boldsymbol{A}$	breakage interaction matrix (Eq. (8))
A_c	column cross-sectional area (m^2)
c_1	coalescence constants (Eq. (17))
c_2	coalescence constants (Eq. (17)) (m^{-2})
$\boldsymbol{d}$	characteristic droplet diameter vector
d, d'	droplet diameter (mm)
d_i	the characteristic droplet diameter in the ith subdomain (mm)
d_{min}, d_{max}	minimum and maximum droplet diameters (mm)
D_c, D_d	diffusion coefficients for the m^2 continuous and dispersed phases, respectively ($m^2\ s^{-1}$)
D_R, D_s	rotor and stator diameters, respectively (m)
$f(v)$	droplet number density function
F	the convective flux ($m^3/m^2\ s$)
H, H_c	column and single compartment heights, respectively (m)
K_v	slowing factor
L	number of external (spatial) coordinate cells

M_x number of subdomain of the internal coordinate (pivots)
n number distribution function (m^{-4})
n^{feed} feed number distribution function (m^{-1})
$N(t, z)$ total droplets number concentration at time t and location z
N^* rotor speed (rpm)
$\boldsymbol{P}$ physical properties vector
P_r breakage probability (Eq. (20))
Q_b total flow rate at bottom of the column ($m^3\,s^{-1}$)
$Q_{c,in}$, $Q_{c,out}$ inlet and outlet continuous phase flow rates ($m^3\,s^{-1}$)
Q_d inlet dispersed phase flow rate ($m^3\,s^{-1}$)
Q_t dispersed phase flow rate at top of the column ($m^3\,s^{-1}$)
t time (s)
u_m any mth property associated with single droplet
U_c continuous phase velocity relative to the column walls ($m\,s^{-1}$)
U_d dispersed phase velocity relative to the column walls ($m\,s^{-1}$)
U_r relative droplet (slip) velocity ($m\,s^{-1}$)
v, v' droplet volumes (m^3)
v_f mean droplet volume of the feed distribution (m^3)
v_{min}, v_{max} minimum and maximum droplet volume (m^3)
x_i the characteristic droplet volume in the ith subdomain (m^3)
z spatial coordinate (m)
z_c continuous phase inlet (m)
z_d dispersed feed inlet (m)

Greek symbols

α_c, α_d as defined in Table 1
β_n daughter droplet distribution based on droplet number (mm^{-1})
$\gamma_i^{\langle i-1\rangle}$, $\gamma_i^{\langle i\rangle}$ triangular functions to satisfy conservation of any two integral properties
Γ droplet breakage frequency (s^{-1})
θ TVD parameter between 1 and 2
$\vartheta(d')$ mean number of daughter droplets produced upon breakage of mother droplet of diameter d'
μ_c continuous phase viscosity ($kg\,m^{-1}\,s^{-1}$)
$\boldsymbol{\rho}$ breakage and coalescence source term
ρ_c, ρ_d density of the continuous and dispersed phases, respectively ($kg\,m^{-3}$)
σ interfacial tension ($N\,m^{-1}$)
ϕ dispersed phase hold-up
ϕ_e dispersed phase hold-up entrained with the continuous phase
$\boldsymbol{\varphi}$ local volume concentration vector whose elements are given by Eq. (5)
$\Psi^{\langle i\rangle}$ the ith coalescence interaction matrix whose elements are given by Eq. (11)
ω coalescence frequency ($m^3\,s^{-1}$)
ω_R, $\omega_{R,crit}$ rotor and critical rotor speeds, respectively (s^{-1})

References

[1] T.C. Lo, M.H.I. Baird, C. Hanson (Eds.), Handbook of Solvent Extraction, John Wiley & Sons, New York, 1983.
[2] V. Jiricny, M. Kratky, J. Prochazka, Counter-current flow of dispersed and continuous phase. I. Discrete polydispersed model, Chem. Eng. Sci. 34 (1979) 1141–1149.
[3] G. Casamatta, Comportement de la population des gouttes dans une colonne d'extraction: transport, rupture, coalescence, transfer de matiere, Dissertation, Institut National Polytechnique De Toulouse, 1981.
[4] M.M. Attarakih, H.-J. Bart, N.M. Faqir, Solution of the population balance equation for liquid-extraction columns using a generalized fixed-pivot and central difference scheme, in: A. Kraslawski, I. Turunen (Eds.), Proceedings of the European Symposium on Computer Aided Process Engineering-13, Computer-Aided Chemical Engineering 14, Elsevier, Amsterdam, 2003, pp. 557–562.
[5] C. Hwang, Y.-P. Shih, Solution of population balance equations via block pulse functions, Chem. Eng. J. 25 (1982) 39–45.
[6] M.M. Attarakih, H.-J. Bart, N.M. Faqir, Numerical solution of the spatially distributed population balance equation describing the hydrodynamics of interacting liquid–liquid dispersions, Chem. Eng. Sci. 59 (2004) 2567–2592.
[7] D. Ramkrishna, Population Balances: Theory and Applications to Particulate Systems in Engineering, Academic Press, San Diego, 2000.
[8] A. Kurganov, E. Tadmor, New high-resolution central schemes for nonlinear conservation laws and convective diffusion equations, J. Comp. Phys. 160 (2000) 241–282.
[9] J.C. Godfrey, M.J. Slater (Eds.), Liquid–Liquid Extraction Equipment, John Wiley & Sons, New York, 1994.
[10] I. Langmuir, The velocity of reactions in gases moving through heated vessels and the effect of convection and diffusion, Z. Phys. Chem. 61 (1988) 422–436.
[11] S.H. Zhang, S.C. Yu, Y.C. Zhou, Y.F. Su, A model for liquid–liquid extraction column performance—the influence of drop size distribution on extraction efficiency, Can. J. Chem. Eng. 63 (1985) 212–226.
[12] T. Kronberger, A. Ortner, W. Zulehner, H.-J. Bart, Numerical determination of droplet size in extraction columns, in: A. Fasano, M. Primerico (Eds.), Proceedings of the Seventh European Conference on Mathematics in Industry, Teubner, Stuttgart, 1994, pp. 247–254.
[13] N.P. Wilburn, Mathematical determination of concentration profiles in two-phase continuous countercurrent extractors, Ind. Eng. Chem. Fundam. 3 (1964) 189–195.
[14] A.J. Klee, R.E. Treybal, Rate of rise or fall of liquid drops, AIChE J. 2 (1956) 444–447.
[15] A. Vignes, Hydrodynamique des dispersions, Genie Chimique 93 (1965) 129–142.
[16] J.R. Grace, T. Wairegi, T.H. Nguyen, Shapes and velocities of single drops and bubbles moving freely through immiscible liquids, Trans. Inst. Chem. Eng. 54 (1976) 167–173.
[17] J.A. Wesselingh, A.M. Bollen, Single particles, bubbles and drops: their velocities and mass transfer coefficients, Trans. Inst. Chem. Eng. 77 (1999) 89–96.
[18] T. Misek, General hydrodynamic design basis for columns, in: J.C. Godfrey, M.J. Slater (Eds.), Liquid–Liquid Extraction Equipment, John Wiley & Sons, Chichester, 1994, pp. 95–113.
[19] H. Hufnagl, M. McIntyre, E. Blass, Dynamic behaviour and simulation of a liquid–liquid extraction column, Chem. Eng. Technol. 14 (1991) 301–306.
[20] O. Weinstein, R. Semiat, D.R. Lewin, Modeling, simulation and control of liquid–liquid extraction columns, Chem. Eng. Sci. 53 (1998) 325–339.

[21] M. Simon, H.-J. Bart, Experimental studies of coalescence in liquid /liquid systems, Chem. Eng. Technol. 25 (2002) 481–484.
[22] M. Simon, S.A. Schmidt, H.-J. Bart, The droplet population balance model—estimation of breakage and coalescence, Chem. Eng. Technol. 26 (2003) 745–750.
[23] C.A. Coulaloglou, L.L. Tavlarides, Description of interaction processes in agitated liquid–liquid dispersions, Chem. Eng. Sci. 32 (1977) 1289–1297.
[24] R. Raman, Chemical Process Computations, Elsevier Applied Science Publishers Ltd., New York, 1985.
[25] Fortran Subroutines for Mathematical Applications, Visual Numerics Inc., Stuttgart, 1997.
[26] G. Modes, Grundsätzliche Studie zur Populationsdynamik einer Extraktionskolonne auf Basis von Einzeltropfenuntersuchungen, Shaker, Aachen, 2000.
[27] S.A. Schmidt, M. Simon, M.M. Attarakih, L. Lagar G., H.-J. Bart, Droplet population balance modelling—hydrodynamics and mass transfer, Chem. Eng. Sci., in press.
[28] L. Steiner, S. Hartland, Neues zur mathematischen Modellierung von Flüssig-Flüssig-Extraktionskolonnen, Chem. Ing. Technol. 55 (3) (1983) 194–201.
[29] J.C. Godfrey, M.J. Slater, Slip velocity relationships for liquid–liquid extraction columns, Trans. IChemE 69 (1991) 130–141.
[30] V. Cauwenberg, J. Degreve, M.J. Slater, The interaction of solute transfer, contaminants and drop break-up in rotating disc contactors. Part I. Correlation of drop breakage probabilities, Can. J. Chem. Eng. 75 (1997) 1046–1055.
[31] V. Alopaeus, J. Koskinen, K.I. Keskinen, J. Majander, Simulation of the population balances for liquid–liquid systems in a nonideal stirred tank. Part 2. Parameter fitting and the use of multiblock model for dense dispersions, Chem. Eng. Sci. 57 (2002) 1815–1825.
[32] V. Alopaeus, J. Koskinen, K.I. Keskinen, Simulation of population balances for liquid–liquid systems in a nonideal stirred tank. Part 1. Description and qualitative validation of model, Chem. Eng. Sci. 54 (1999) 5887–5899.